Available online at www.sciencedirect.com
SCIENCE DIRECT®
International Journal of Multiphase Flow 31 (2005) 548–570
International Journal of Multiphase Flow
www.elsevier.com/locate/ijmulflow

Ethanol–CO_2 two-phase flow in diverging and converging microchannels

J.J. Hwang, F.G. Tseng, Chin Pan *

Department of Engineering and System Science, National Tsing Hua University, Hsinchu, 101, Sect 2, Kuang Fu Road, Hsinchu 30043, Taiwan

Received 22 November 2004; received in revised form 30 January 2005

Abstract

The present study investigates experimentally two-phase flow patterns and pressure drop of ethanol and CO_2 in a converging or diverging rectangular microchannel. The two-phase flow pattern visualization is made possible using a high speed video camera. The increased superficial gas velocity due to the acceleration effect and the large pressure drop in a converging channel may result in the elongation of bubbles in slug flow, while the decreased superficial velocity owing to the deceleration effect and the possible pressure rise in the diverging channel may cause shortening of bubbles in slug flow significantly. For both types of channel, the collision and merger of two consecutive bubbles may take place and result in necking of bubbles. Two-phase flow pressure drop in the converging microchannel increases approximately linearly with the increasing liquid or gas flow rate with the frictional pressure drop being the major contributor to the channel pressure drop. In the diverging microchannel, the deceleration effect results in the pressure rise and counteracts the frictional pressure drop. Consequently, for low liquid flow rates the channel pressure drop increases only slightly with the gas flow rate while it is low and a reversed trend appears while it is high. For high liquid flow rates the effect of increasing gas flow rate on channel pressure drop is much more significant; a more significant reverse trend of the effect of gas flow rate is present in the region of high gas flow rates. The two-phase frictional multiplier in the converging or diverging microchannel is quite insensitive to the liquid flow rate and can be fitted very well within ±15% based on the Lockhart–Martinelli

* Corresponding author. Tel.: +886 35 715131; fax: +886 35 720724.
E-mail address: cpan@ess.nthu.edu.tw (C. Pan).

0301-9322/$ - see front matter
doi:10.1016/j.ijmultiphaseflow.2005.01.011

equation with a modified Chisholm parameter for the diverging microchannel and together with a modified coefficient for the X^{-2} term for the converging microchannel.

1. Introduction

The two-phase flow in microchannels is of fundamental importance for many interesting applications, such as boiling heat transfer in a compact heat exchanger, CO_2 bubble removal in a micro direct methanol fuel cell, and blood flow through small capillaries. Two-phase flow patterns, bubble speed, void fraction, two-phase flow pressure drop and boiling heat transfer are those of significant interest.

Recently, there have been very active research activities on gas–liquid two-phase flow in minichannels or microchannels. For example, Fukano and Kariyasaki (1993) and Mishima and Hibiki (1996) studied air/water two-phase flow pressure drop in minichannels. Mishima and Hibiki found that the two-phase frictional multiplier may be predicted well by the Lockhart–Martinelli correlation with the Chisholm's parameter C decreasing with decreasing channel diameter in the following way:

$$\Phi_{\mathrm{L}}^2 = 1 + \frac{C}{X} + \frac{1}{X^2} \tag{1}$$

$$C = 21(1 - \mathrm{e}^{-0.319 D_{\mathrm{H}}}) \tag{2}$$

where Φ_{L}^2 is the two-phase frictional multiplier, X is the Lockhart–Martinelli parameter, and D_{H} is the hydraulic diameter of the channel. Triplett et al. (1999a,b) investigated air/water two-phase flow patterns, void fraction and two-phase flow pressure drop in minichannels. They reported that for bubbly and slug flows the experimental two-phase frictional pressure drop data agree reasonably well with the predictions of a homogeneous mixture model with a mixture viscosity at high Reynolds numbers, while at low Reynolds numbers or for annular flow, both the homogeneous mixture model and Friedel's correlation predict the data poorly. Chen et al. (2002) investigated experimentally nitrogen/water two-phase flow pattern, bubble speed and void fraction in a glass capillary (minichannel). In addition to bubbly, slug, churn and annular flow, they reported a special flow pattern called "bubble-train slug flow" with a detailed analysis. In such a flow pattern, typically two to four bubbles, and possibly up to ten or more, could connect together, resembling a train, with a clear interface between connecting bubbles. Moreover, using the high speed video camera, they were able to measure the bubble speed accurately. With both the bubble speed and superficial gas velocity measured, the void fraction can be determined accurately according to its basic definition. A correlation for void fraction was also developed.

Stanley et al. (1997) studied two-phase flow of water and gas (argon, helium or nitrogen) in rectangular microchannels. They found that the two-phase frictional multiplier was significantly influenced by the physical dimensions of the channel such as relative roughness, length to diameter ratio and aspect ratio, and quality in terms of $(1 - x)/x$. Kawahara et al. (2002) investigated

nitrogen/water two-phase flow in a quartz capillary with an inner diameter of 100 μm. Two-phase flow pattern, void fraction and two-phase flow pressure drop were studied. A correlation for void fraction in a microchannel was developed based on volumetric quality and the two-phase friction multiplier data were found to be in good agreement with the conventional correlations. Serizawa et al. (2002) explored air/water two-phase flow in circular tubes of 20, 25 and 100 μm. Several distinctive flow patterns were reported and the flow pattern was found to be sensitive to the surface conditions. Chung and Kawaji (2004) investigated the effect of channel diameter on water/nitrogen two-phase flow in circular microchannels of 530, 250, 100 and 50 μm diameters. It was found that the two-phase flow characteristics in channels of 100 and 50 μm are different from those in mini-channels in many ways such as slug flow becoming dominant, significant slip between gas and liquid and insignificant effect of mass flux on two-phase flow frictional multiplier.

The present study investigates experimentally the characteristics of ethanol/CO_2 two-phase flows in a converging or diverging rectangular microchannel. This work is motivated by the need to remove the CO_2 bubbles produced in the anode of a micro direct methanol fuel cell (DMFC). Bubbles of carbon dioxide are inevitably produced in the anode due to the oxidation of methanol. Its removal is of critical importance as CO_2 bubbles may block the fueling channel (Argyropulos et al., 1999) and significantly influence the performance of a micro DMFC. Lee et al. (2004) have found that bubble departure in a uniform boiling microchannel is governed by the surface tension and the drag due to bulk two-phase flow. Due to acceleration or deceleration effects, two-phase flow characteristics in a converging or diverging microchannel may be significantly different from that in a microchannel with uniform cross section. In the literature, Lin et al. (1994) reported the bubble movement in a short divergent microchannel. They attributed the movement of the bubble to a large cross section to be caused by interfacial tension force. The objectives of the present study are to explore the two-phase flow characteristics in a converging or diverging microchannel. Therefore, the advantages and disadvantages of using a microchannel with variable dimensions for the transport of a gas–liquid mixture may be examined. Two-phase flow patterns and pressure drop in a converging or diverging channel are investigated. The present study employs ethanol to simulate methanol.

2. Experimental detail

2.1. Experimental setup

A schematic diagram of the experimental setup, consisting of the test section with a converging or diverging rectangular microchannel, gas mass flow controller, high performance liquid chromatography pump (HPLC pump), flow visualization system and pressure measurement system, is shown in Fig. 1. The top and side views of the test section are illustrated in Fig. 2(a) and (b). The converging microchannel width varied linearly from 1575 μm to 45 μm and from 35 μm to 1475 μm for the diverging one. The length for both types of channel was 20 mm. Therefore, the converging and diverging wall angles for both channels were 2.19° and 2.06°, respectively. The channel depths were 69.5 μm and 59.6 μm for converging and diverging channels, respectively. Thus, the hydraulic diameters for the converging channel at the inlet and outlet were 133 μm and 54.6 μm, respectively, and for the diverging channel 44.1 μm and 115 μm at the inlet

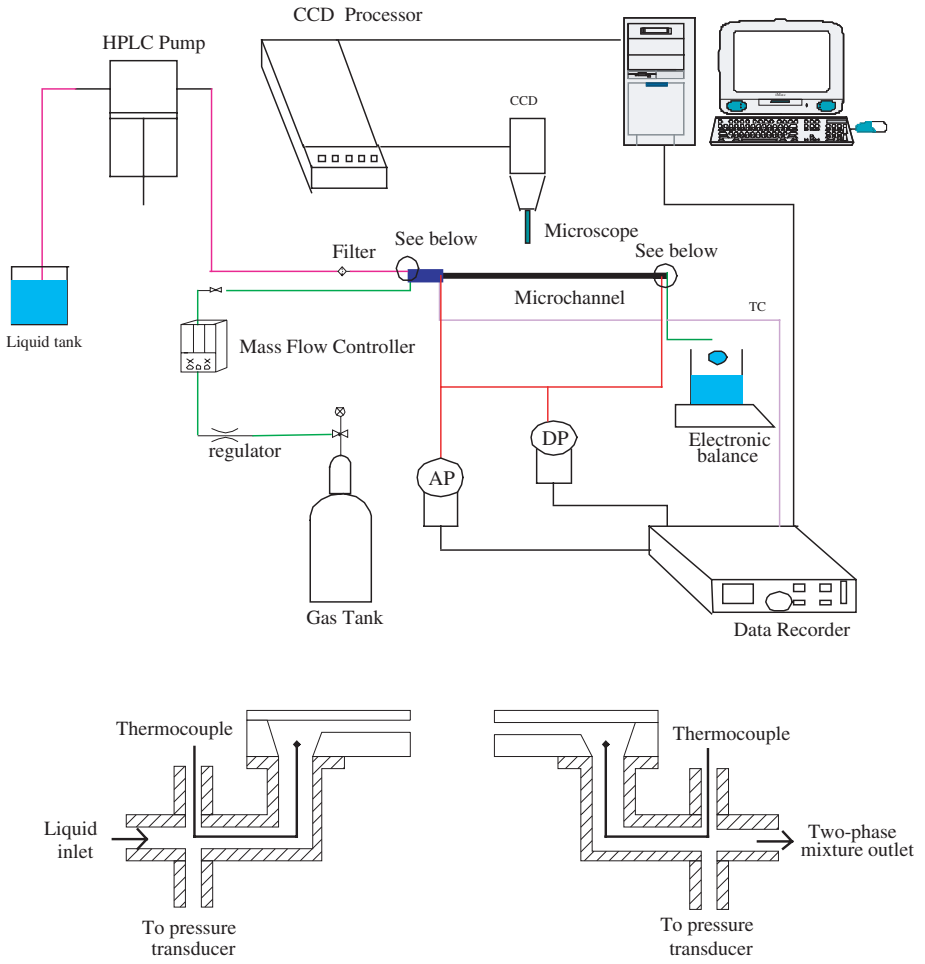

Fig. 1. A schematic diagram of the experiment setup.

and outlet, respectively. The mean diameters for both channels were 122 and 105 μm, respectively, based on the following definition:

$$D_{\mathrm{H,m}} = \frac{1}{L}\int_0^L D_{\mathrm{H}}(z)\mathrm{d}z = \frac{2H}{L}\int_0^L \frac{W(z)}{H+W(z)}\mathrm{d}z = 2H\left[1 - \frac{H}{W_{\mathrm{ex}} - W_{\mathrm{in}}}\ln\frac{H+W_{\mathrm{ex}}}{H+W_{\mathrm{in}}}\right] \tag{3}$$

where $D_{\mathrm{H}}(z)$ is the local hydraulic diameter at z, the axial distance from inlet; H is the channel height; L is the channel length; and $W(z)$ is the local channel width, W_{in} and W_{ex} stand for channel width at the inlet and exit, respectively. The top surface dimension of the test section was 7 mm × 35 mm.

The carbon dioxide flow rate was controlled by a mass flow controller ranging from 0 to 20 SCCM. The HPLC pump provided a constant flow of ethanol (95% ethanol + 5% water) in the microchannel. The flow range of the HPLC pump was from 0.01 ml/min to 10.0 ml/min. A filter with a mesh size of 0.1 μm was installed in front of the inlet of the microchannel. Carbon dioxide

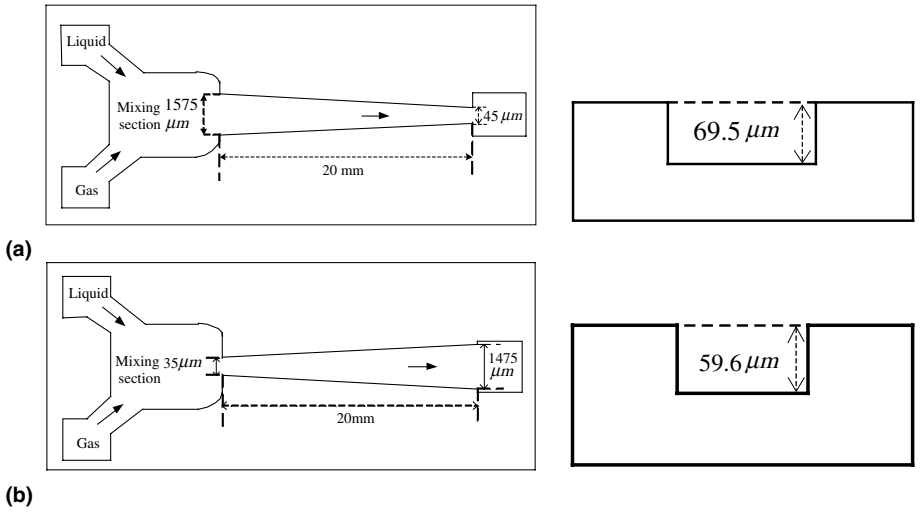

Fig. 2. The top and side views of the test section in (a) convergent, (b) divergent microchannel (length shown not to scale).

and ethanol entered the mixing section from each corner of the end side, as shown in Fig. 2. The liquid flow rate given by the pump was calibrated by using an electronic balance. The liquid of the gas–liquid mixture discharged from the microchannel outlet was collected in a small narrow-mouthed container over a sufficient time and subsequently the liquid weight was measured to determine the flow rate. The container was exposed to atmosphere and, therefore, the pressure at the channel outlet remained at nearly the atmospheric pressure.

The absolute pressure in front of the channel inlet and the differential pressure between the inlet and outlet of the microchannel were measured using pressure transducers. As shown in the inserts of Fig. 1, the pressure taps were located at the connecting tubes right before the channel inlet or outlet. The temperatures at the inlet and outlet were detected by T-type thermocouples. The outputs of pressure transducers and thermocouple were recorded by a data acquisition system (YOKOKAWA AR 1100A).

The flow visualization system included a high-speed digital camera (KODAK motion coder SR-ultra), a monitor and a personal computer. To observe the two-phase flow pattern in the diverging and converging microchannels, a micro-lens was mounted on the CCD. Typically the frame rate was set at 2000 frame/s and the shutter speed at 1/5000 s. An x–y–z translation stage was installed with the test module to hold the lens and provide accurate positioning along the test plane (x–y plane) and focusing (z-direction).

2.2. Fabrication of the test section

The test section was a 7 mm × 35 mm silicon strip, sliced from P-type ⟨100⟩ orientation wafer. The fabrication process of the microchannels employed bulk micromachining and anodic bonding process. The process began with the passivation of 1 μm low stress silicon nitride using low pressure chemical vapor deposition (LPCVD). Subsequently, the microchannel and mixing section

were etched by using deep silicon reactive ion etching (DSRIE). To enable flow visualization, the top surface was covered with Pyrex 7740 glass through anodic bonding. Finally, a KOH etch from the back was employed for the through holes to the inlet and outlet regions, respectively.

2.3. Experimental procedure

The present study employed ethanol and carbon dioxide as the working fluids. The pressure drop of single-phase liquid flow was measured at a specific flow rate. Subsequently, the gas volume flow rate was varied with the liquid flow rate fixed to precede two-phase flow experiments. Thereafter, the liquid flow rate was changed and the single- and two-phase experiments were repeated. The volume flow rates of ethanol and carbon dioxide were controlled to range from 3.18×10^{-9} m^3/s to 1.64×10^{-8} m^3/s and from 1.50×10^{-8} m^3/s to 1.80×10^{-7} m^3/s, respectively. Two-phase flow pressure drop through both types of channel was measured. Moreover, a high-speed video camera was employed to capture the variation of two-phase flow patterns in both diverging and converging microchannels.

2.4. Measurement uncertainty

The measurement uncertainties for ethanol mass flow rate in diverging and converging microchannels were estimated to be 3.85% and 1.75%, respectively. The measurement uncertainty in carbon dioxide volume flow rate was 1%. The measurement uncertainty of pressure transducer was 0.1% and response time was 0.2 s.

3. Results and discussion

3.1. Two-phase flow patterns

Two-phase flow patterns in a convergent or divergent microchannel could significantly change while the fluid flowed downstream due to the effects of fluid acceleration or deceleration and pressure variations. Fig. 3 illustrates the effect of gas flow rate on the evolution of the two-phase flow pattern in a converging channel at a liquid flow rate of 8.23×10^{-9} m^3/s. In this figure and later in Fig. 4, Figs. 6 and 7, regions 1 and 4 are located immediately next to the inlet and outlet, respectively, as clearly illustrated, while regions 2 and 3 are those regions at about one third and two thirds, respectively, of channel length form the inlet. The figure demonstrates bubbly flow near the entrance i.e., the region 1, at a very low gas flow rate of 3.00×10^{-8} m^3/s at the inlet. The figure also shows that the strong liquid flow pushes the gas flow toward the upper wall in the figure near the entrance. With an increase in the gas flow rate, the gas flow at and near the entrance becomes continuous and a wavy stratified flow is formed there. The two-phase flow pattern evolves to slug flow or slug-annular flow while flowing downstream due to the acceleration effect caused by area contraction. The superficial velocities of both liquid and gas phases are significantly increased in the downstream regions due to large reduction in channel cross section. Such a greatly increased superficial gas velocity may elongate the bubble. Moreover, the large pressure drop along the bubble may also have the similar effect due to bubble expansion.

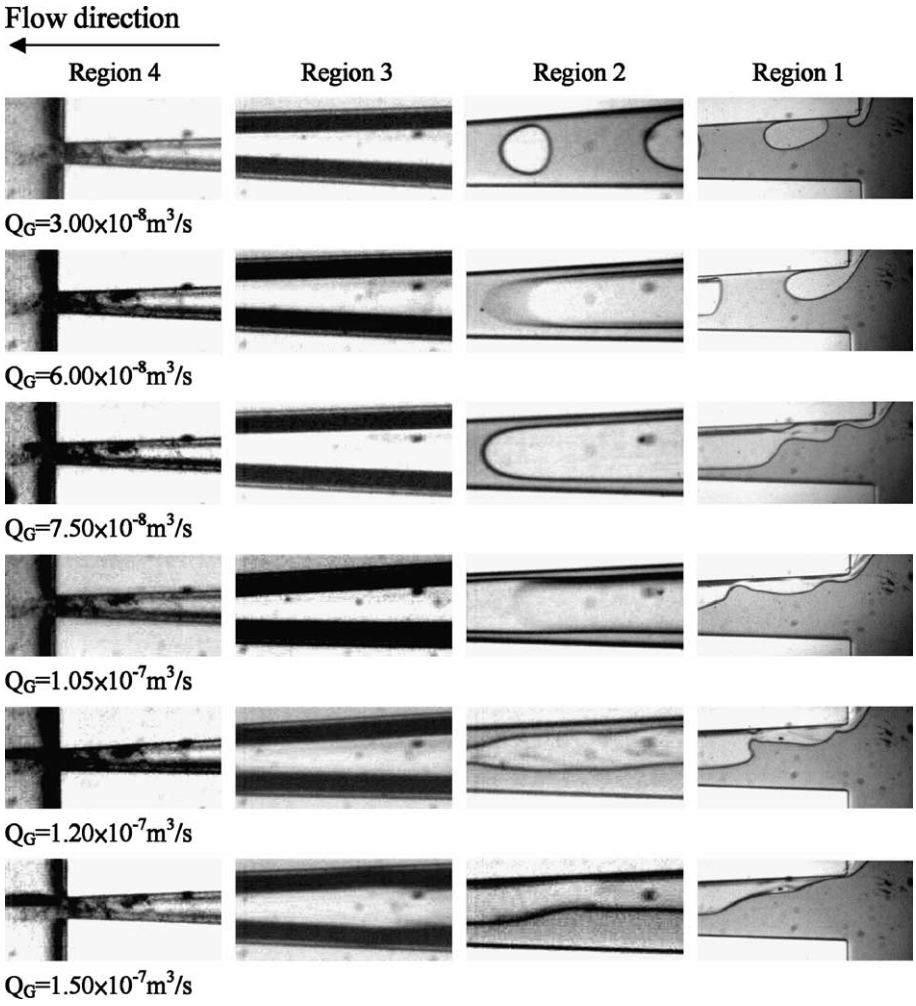

Fig. 3. Effect of gas flow rate on the evolution of two-phase flow pattern in the converging microchannel at a constant liquid flow rate ($Q_L = 8.23 \times 10^{-9}$ m^3/s).

Fig. 4 shows the effect of liquid flow rate on the variation of two-phase flow pattern in the converging channel for a gas flow rate of 1.20×10^{-7} m^3/s. For such a high gas flow rate, wavy stratified flow is formed near the entrance. For low liquid flow rates slug flow or slug-annular flows are formed in the downstream regions. For higher liquid flow rates, the gas tends to flow in the middle part of channel shortly after it enters the channel. Strong interactions between gas and liquid flows results in a peculiar flow pattern which can be found in the region next to the entrance for $Q_L \geqq 8.23 \times 10^{-9}$ m^3/s. Such a peculiar two-phase flow pattern is a special form of churn flow due to the collision and merger of two bubbles in slug flow as demonstrated in Fig. 5 for another set of experimental conditions i.e., $Q_G = 9.00 \times 10^{-8}$ m^3/s and $Q_L = 8.23 \times 10^{-9}$ m^3/s. Due to the acceleration effect, the leading bubble is longer and, therefore, may experience a larger drag than the follower and it could travel slower than the following one leading to bubble collision. Fig. 5

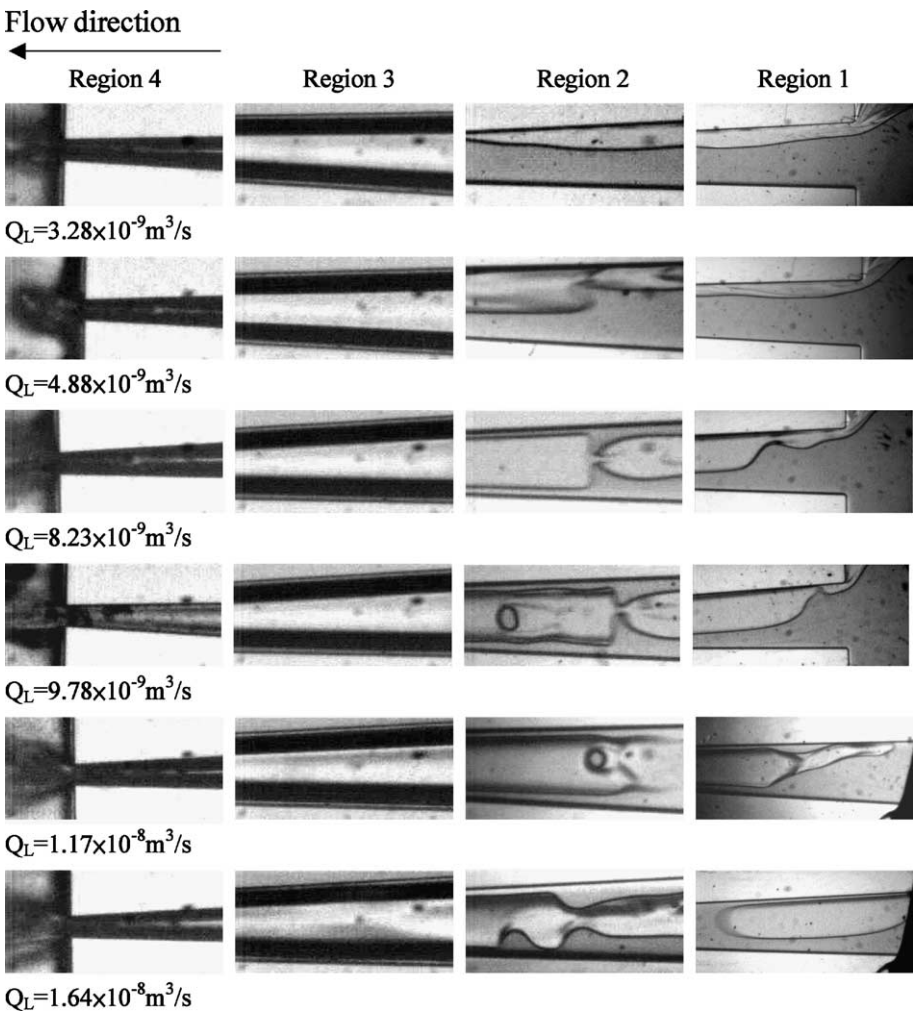

Fig. 4. Effect of liquid flow rate on the evolution of two-phase flow pattern in the converging microchannel at a constant gas flow rate ($Q_G = 1.20 \times 10^{-7}$ m^3/s).

shows that at $t + 1.5$ ms ($t + 3/2000$). A little "eye" shaped liquid bridge is left at the junction of two bubbles. At $t + 7$ ms ($t + 14/2000$), a necking bubble is formed. Such a necking bubble due to the collision of two elongated bubbles in slug flow is unique in such a converging channel. In a uniform minichannel, such a kind of bubble interaction may result in the formation of bubble train slug flow (Chen et al., 2002), i.e., the interface between two connecting bubbles remains intact.

Fig. 6 displays the effect of liquid flow rate on the evolution of two-phase flow pattern in the diverging channel for a gas flow rate of 1.50×10^{-8} m^3/s. Slug flow with very long bubble, prevails for both regions near the entrance, i.e., regions 1 and 2. The figure clearly exhibits that the decrease of the superficial gas velocity and the pressure rise due to deceleration effect shortens the bubble length in the regions 3 and 4 for low liquid flow rates. Moreover, the bubble head

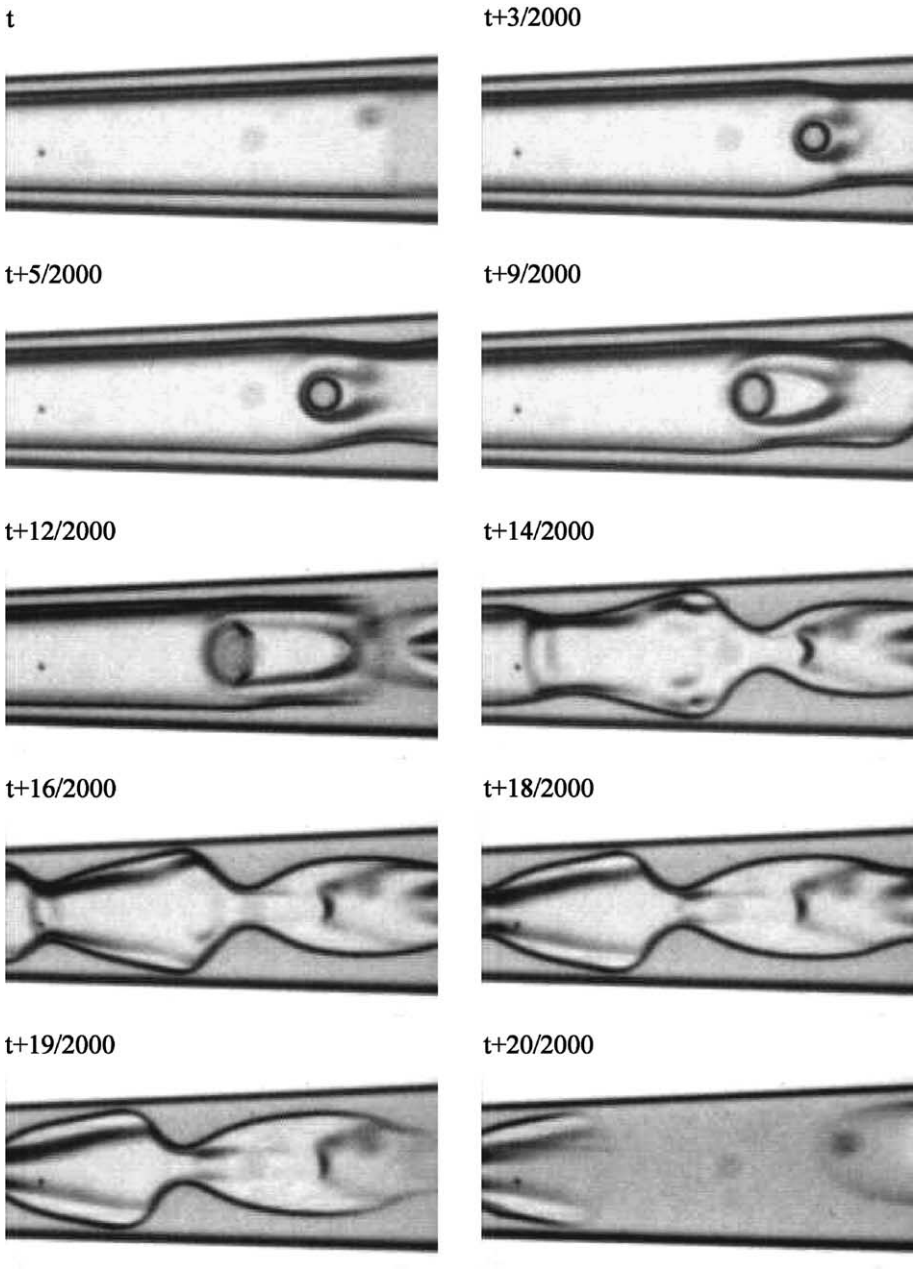

Fig. 5. Churn flow in converging microchannel with $Q_G = 9.00 \times 10^{-8}$ m^3/s and $Q_L = 8.23 \times 10^{-9}$ m^3/s.

becomes very sharp with a tip while it is reaching the exit of the channel indicating the high pressure there and the presence of reversed liquid flow near the wall possibly due to the boundary layer separation effect. Interestingly, for a liquid flow rate of 9.67×10^{-9}m^3/s and 1.13×10^{-8} m^3/s, the bubbles in the region 3 are so short that the flow pattern becomes bubbly rather

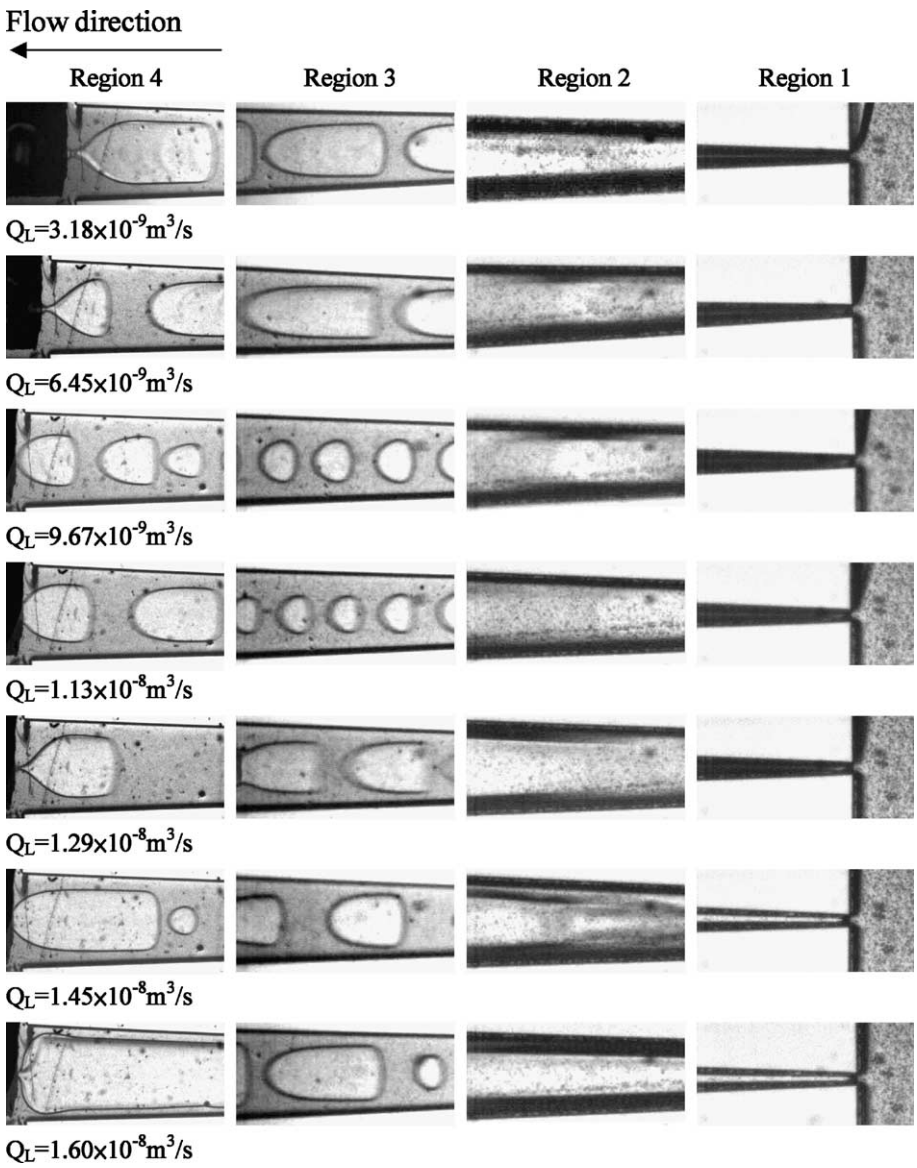

Fig. 6. Effect of liquid flow rate on the evolution of two-phase flow pattern in the diverging microchannel at a constant gas flow rate ($Q_G = 1.50 \times 10^{-8}$ m^3/s).

than slug flow. For those two particular cases, the bubble becomes longer again when it flows to the region 4, possibly due to the merger of bubbles. For the liquid flow rate equal or greater than 1.29×10^{-8} m^3/s, the flow pattern in the region 3 becomes slug flow again. Sometimes, it becomes multiple flow patterns with a long bubble followed by a small bubble. The bubble at the exit region becomes very long if the liquid flow rate is further increased to 1.60×10^{-8} m^3/s. A sharp tip on the bubble head is also present for this case.

The effect of gas flow rate on the evolution of two-phase flow pattern in a diverging channel at a liquid flow rate of 4.77×10^{-9} m^3/s is shown in Fig. 7. The region between the vertical wall and the dark band in the inlet mixing region is due to the gas flow. The figure demonstrates annular-slug flow for both regions near the entrance, i.e., region 1 and region 2 for various different gas flow rates. As for the regions near the exit, the two-phase flow pattern becomes more complicated for high gas flow rates. For the case with the lowest flow rate, i.e. $Q_G = 3.00 \times 10^{-8}$ m^3/s, no bubble collisions take place in the region 3 or 4. The sharp bubble head at the exit indicates the possible presence of reversed flow. For $Q_G \geqq 9.00 \times 10^{-8}$ m^3/s, bubble collisions occur. The interactions could be very violent and a new bubble with necking is formed as the gas flow rate is further increased.

Fig. 8 demonstrates the collision and merger process for such a case at $Q_G = 4.50 \times 10^{-8}$ m^3/s and $Q_L = 6.56 \times 10^{-9}$ m^3/s near the exit. The liquid flow rate for this case is greater than that for Fig. 7. At time t the follower, which is somewhat longer and thinner than the leading one, is very close to the leading bubble. At 1 ms later, the follower actually hits the leading bubble. At $t + 2$ ms, the two bubbles merge together and a large bubble with a dumbbell shape is formed.

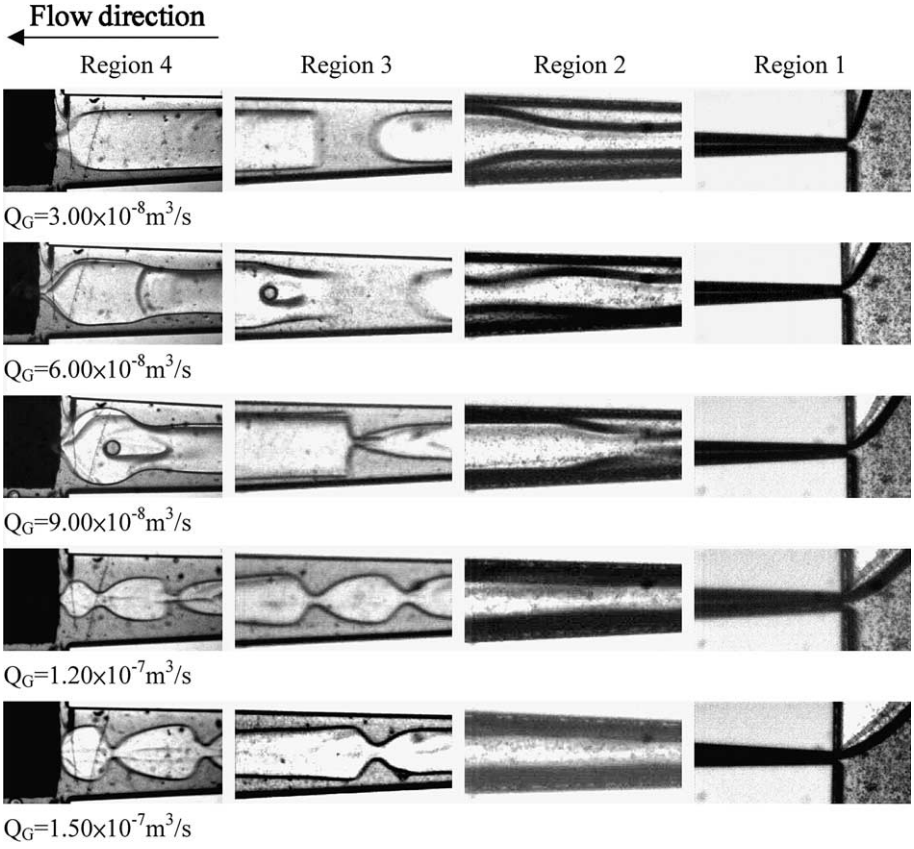

Fig. 7. Effect of gas flow rate on the evolution of two-phase flow pattern in the diverging microchannel at a constant liquid flow rate ($Q_L = 4.77 \times 10^{-9}$ m^3/s).

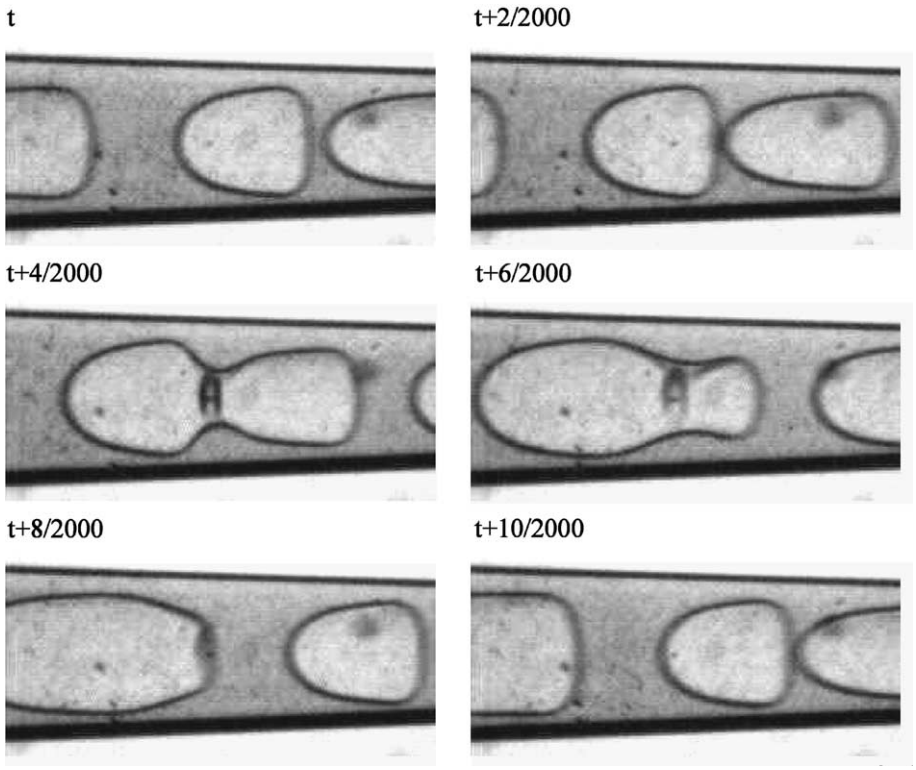

Fig. 8. Bubble collision and merger in the diverging microchannel at $Q_G = 4.50 \times 10^{-8}$ m^3/s and $Q_L = 6.56 \times 10^{-9}$ m^3/s.

Another 1 ms later, the bubble becomes paramecium-like. At $t + 5.0$ ms, a large bubble with a round head and near-flat rear end is formed. Another collision of two bubbles occurs and merger begins. In the diverging channel, the leading bubble may move slower than the follower due to the deceleration effect. Consequently, the follower may hit the leading one and results in the merger of the two bubbles.

Fig. 9 illustrates another kind of bubble collision in a diverging channel near the exit with $Q_G = 1.50 \times 10^{-7}$ m^3/s and $Q_L = 6.56 \times 10^{-9}$ m^3/s. For this case, the liquid flow rate is the same as in the previous case, while the gas flow rate is much larger than in the previous case. The collision of two bubbles causes the necking of the resulting bubble similar to that shown in Fig. 5 for the converging channel. However, the slowing down mechanism of the leading bubble is different for both cases as discussed previously.

3.2. Single-phase flow pressure drop

Fig. 10(a) and (b) illustrate the total pressure drop, channel pressure drop, frictional pressure drop, acceleration pressure drop, and inlet and outlet pressure loss for single-phase liquid flow through the converging and diverging microchannels, respectively. The inlet and outlet pressure

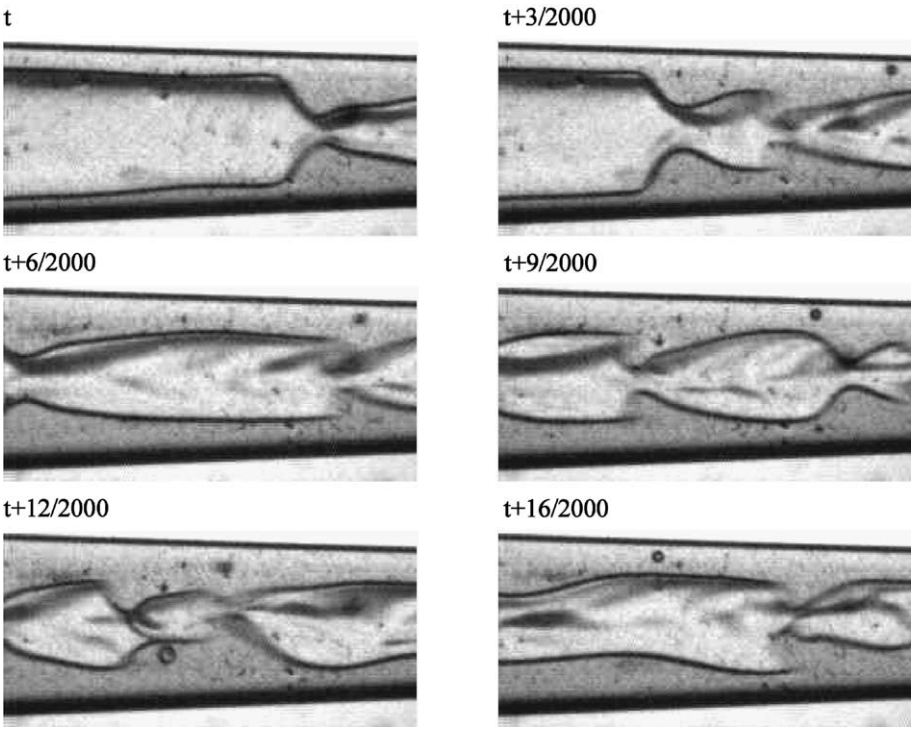

Fig. 9. Bubble collision and merger in the diverging microchannel near the exit at $Q_G = 1.50 \times 10^{-7}$ m^3/s and $Q_L = 6.56 \times 10^{-9}$ m^3/s.

drops account for the pressure loss due to sudden contraction and sudden expansion and may be evaluated approximately by the following equation

$$\Delta P_{loss} = k \frac{1}{2} \rho_L V^2, \tag{4}$$

where ρ_L is the liquid density and k is a loss coefficient based on the velocity head (V) in the small channel (White, 1979)

$$k = \begin{cases} [1 - A_{12}]^2, & \text{sudden expansion} \\ 0.42[1 - A_{12}], & \text{sudden contraction} \end{cases} \tag{5}$$

where

$$A_{12} = A_1/A_2, \tag{6}$$

A_1 = cross sectional area just before the expansion or after the contraction, and A_2 = cross sectional area just before the contraction or after the expansion.

The pressure loss from the measuring point to the inlet or outlet is very small and neglected as the connecting tubes are short and have a much larger cross section than the microchannel.

The channel pressure drop is the balance between total pressure drop and inlet/outlet pressure loss,

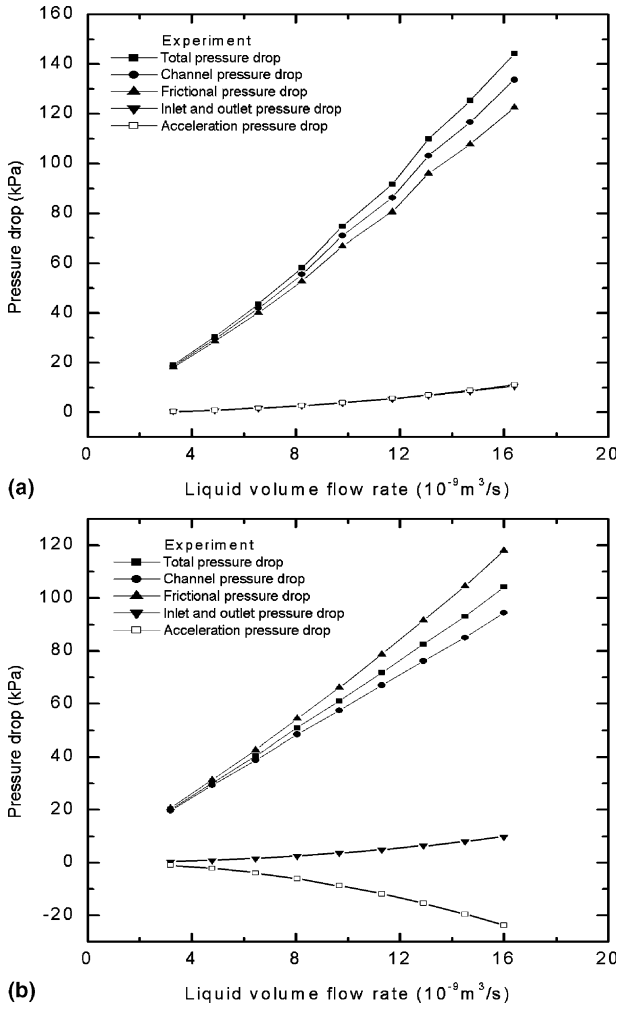

Fig. 10. Various components of single-phase pressure drop in the (a) converging and (b) diverging microchannel.

$$\Delta P_{\mathrm{ch}} = \Delta P_{\mathrm{tot}} - \Delta P_{\mathrm{loss}} \tag{7}$$

The channel pressure drop consists of acceleration and frictional contributions:

$$\Delta P_{\mathrm{ch}} = \Delta P_{\mathrm{a}} + \Delta P_{\mathrm{f}} \tag{8}$$

$$\Delta P_{\mathrm{a}} = \frac{1}{2}\rho_{\mathrm{L}}(V_{\mathrm{ex}}^2 - V_{\mathrm{in}}^2) \tag{9}$$

where V_{ex} and V_{in} are the velocity at the channel exit and inlet, respectively.

$$\Delta P_{\mathrm{f}} = \int_0^L \frac{1}{2}\rho_{\mathrm{L}} V^2(z) f \frac{1}{D_{\mathrm{H}}(z)}\mathrm{d}z \tag{10}$$

where the friction factor may be evaluated by the Hagen–Poiseuille equation:

$$f = \frac{C(z)}{Re(z)} = \frac{\mu_L C(z)}{\rho_L V(z) D_H(z)} \tag{11}$$

where $Re(z)$ is the local Reynolds number at z and μ_L is the liquid viscosity.

In the converging channel, as shown in Fig. 10(a), the acceleration pressure drop is positive, but it is as insignificant as the inlet/outlet pressure loss. The frictional pressure drop is dominant. The maximum frictional pressure drop is around 120 kPa for a liquid flow rate of 1.64×10^{-8} m^3/s. Fig. 10(b) shows that the deceleration effect causes a negative acceleration pressure drop in the diverging channel. The maximum value of the acceleration pressure drop is around 23 kPa for a liquid flow rate of 1.60×10^{-9} m^3/s. The frictional pressure drop is, again, most dominant and increases approximately linearly with the increasing liquid flow rate with a maximum of about 120 kPa for a liquid flow rate of 1.60×10^{-9} m^3/s. Due to the negative acceleration pressure drop, both the total pressure drop and channel pressure drop are smaller than the frictional pressure drop.

Yang et al. (2003) have found that Eqs. (10) and (11) may reasonably predict the frictional pressure drop in a micro nozzle and diffuser. For the present study, the Reynolds number for the converging channel ranges from 1.39 to 12.9 at the inlet and from 20.0 to 186 at the exit, while for the diverging channel the Reynolds number ranges from 10. 6 to 52.9 at the inlet and from 27.4 to 137 at the exit. Therefore, for the present study, laminar flow prevails in both converging and diverging channels and the application of Eq. (11) should be acceptable. Fig. 11(a) and (b) demonstrates that the theoretical predictions based on Eq. (11) agree with experimental data fairly well with a constant value of $C = 160$ in the converging channel and $C = 91.4$ in the diverging channel. For both types of channel, the theory over-predicts the pressure drop for low liquid flow rates and under-predicts for high flow rates. The agreement for the diverging channel is better than that for the converging channel.

3.3. Two-phase flow pressure drop

In the present study, the total two-phase flow pressure drops under various different flow rate conditions are measured. Similar to that for the single-phase liquid flow pressure drop, the channel pressure drop is the balance of total pressure drop and inlet/outlet pressure loss. For two-phase flows, the inlet and outlet pressure loss due to sudden contraction and expansion may be evaluated by the following two equations (Collier and Thome, 1994)

$$\Delta P_{\text{in, 2p}} = \frac{1}{2} G^2 \frac{1}{\rho_L} \left[1 - \frac{1}{A_{12}^2}\right] \left[\frac{(1-x)^2}{(1-\alpha)^2} + \frac{\rho_L}{\rho_G} \frac{x^2}{\alpha^2}\right] \tag{12}$$

$$\Delta P_{\text{ex, 2p}} = -G^2 \frac{1}{\rho_L} A_{12}(1 - A_{12}) \left(\frac{\rho_L}{\rho_G} \frac{x^2}{\alpha} + \frac{(1-x)^2}{1-\alpha}\right) \tag{13}$$

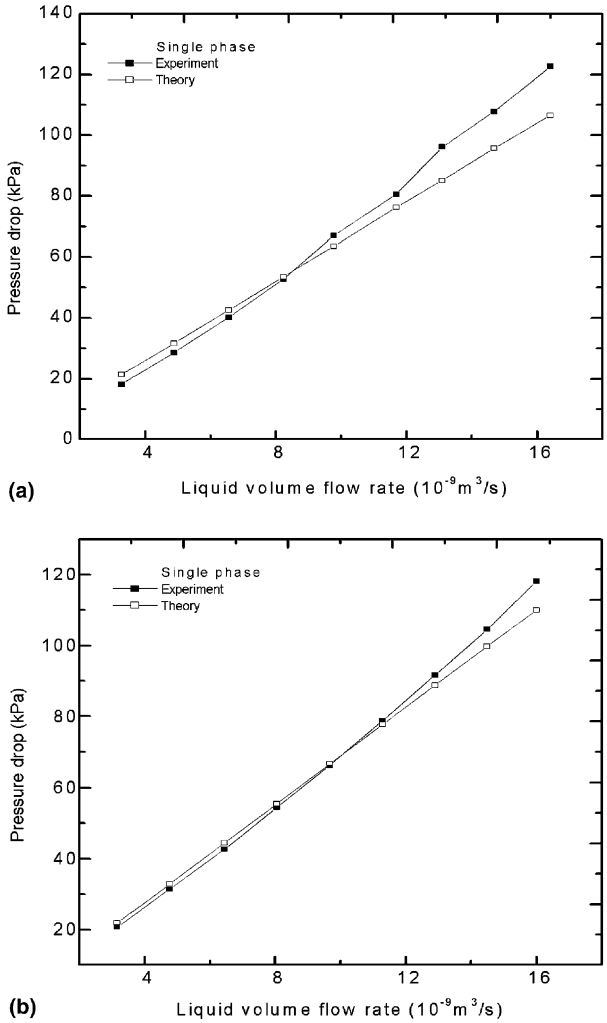

Fig. 11. Comparison of the experimental single-phase frictional pressure drop with theory in the (a) converging, and (b) diverging microchannel.

where G is the mass flux based on the velocity head in the small channel, x is the gas quality, α is the void fraction, and ρ_G represents the gas density. Equation (12) neglects the possible frictional loss for enlargement from vena contracta to the channel wall after sudden contraction.

The channel pressure drop consists of two components: acceleration and frictional pressure drops. The acceleration pressure drop can be obtained by the integration of the following equation from the two-fluid model:

$$-\left(\frac{dP}{dz}\right)_{a,2p} = \frac{d}{dz}[\rho_L(1-\alpha)w_L^2 + \rho_G\alpha w_G^2] \tag{14}$$

Thus,

$$\Delta P_{a,2p} = \int_0^L -\left(\frac{dP}{dz}\right)_{a,2p} dz = \frac{m_L^2}{\rho_L}\left[\frac{1}{A_{ex}^2(1-\alpha_e)} - \frac{1}{A_{in}^2(1-\alpha_{in})}\right] + \frac{m_G^2}{\rho_G}\left[\frac{1}{A_{ex}^2\alpha_e} - \frac{1}{A_{in}^2\alpha_{in}}\right] \tag{15}$$

where m_L and m_G represent the liquid and gas mass flow rate, respectively. The gas density is evaluated at room temperature and average pressure between channel inlet and outlet. The void fractions in above equations are evaluated by the equation proposed by Kawaji and his co-workers (Kawahara et al., 2002):

$$\alpha = \frac{0.03\beta^{0.5}}{1 - 0.97\beta^{0.5}} \tag{16}$$

where β is the volume quality defined as:

$$\beta = \frac{j_G}{j_G + j_L} \tag{17}$$

where j_G and j_L are superficial gas and liquid velocities, respectively.

The frictional pressure drops of two-phase flow though the converging or diverging channel can then be obtained by the following equation.

$$\Delta P_{f,2p} = \Delta P_{ch,2p} - \Delta P_{a,2p} \tag{18}$$

Fig. 12(a) and (b) illustrate the total pressure drop measured and the channel pressure drop evaluated as a function of gas and liquid flow rates in a converging channel, respectively. Both the total and channel pressure drops increase with increasing gas or liquid flow rate. There seems to be a significant variation in pressure drop for the liquid flow rate changing from 8.23×10^{-9} m^3/s to 9.78×10^{-9} m^3/s, especially for gas flow rates between 6.00×10^{-8} m^3/s and 1.50×10^{-7} m^3/s. However, flow visualization does not show significant change in two-phase flow pattern (see Fig. 4).

Fig. 13 exhibits the contributions of various different components of pressure drop or loss as a function of gas flow rate for $Q_L = 9.78 \times 10^{-9}$ m^3/s. The figure indicates that the inlet/outlet pressure loss is insignificant for the range of gas flow rate of the present study. The contribution of acceleration pressure drop to the total pressure chop is about 11% to 24%. The frictional pressure drop is most dominant as one may expect.

Fig. 14(a) and (b) illustrates the effects of gas and liquid flow rates on the total and channel pressure drops in the diverging microchannel. In general, the total pressure drop increases with increases in gas or liquid flow rate. As for the channel pressure drop, the effect of gas flow rate is quite insignificant especially for the cases with low liquid flow rates ($Q_L \leqslant 6.45 \times 10^{-9}$ m^3/s). The channel pressure drop slightly increases with gas flow rate for low gas flow rates while it slightly decreases with gas flow rate for high gas flow rates. For $Q_L > 6.45 \times 10^{-9}$ m^3/s, the increasing effect of gas flow rate on channel pressure drop in the region of low gas flow rate is much more significant. Moreover for the cases of high liquid flow rates and low gas flow rates, a reversed trend of liquid flow rate on the channel pressure drop is present: at a given gas flow rate, a higher liquid flow rate may actually result in a lower channel pressure drop. Significantly,

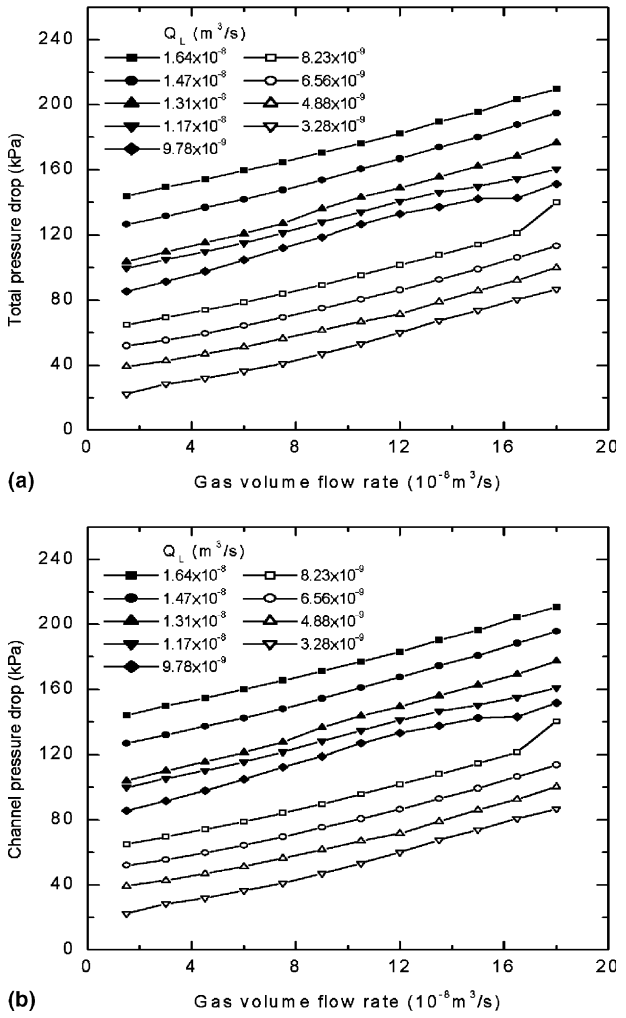

Fig. 12. Two-phase pressure drop in the converging channel (a) total pressure drop, and (b) channel pressure drop.

for high liquid flow rates, the channel pressure drop decreases with an increase in gas flow rate after it reaches a maximum.

The decreasing effect of channel pressure drop at high gas flow rate is caused by the deceleration effect in the diverging channel. Fig. 15 illustrates the contribution of various components of pressure drop/loss in the diverging channel at $Q_L = 8.05 \times 10^{-9}$ m^3/s as a function of gas flow rate. The figure indicates that the magnitude of negative acceleration pressure drop due to the deceleration effect increases with the increasing gas flow rate. For $Q_G = 1.80 \times 10^{-7}$ m^3/s, the pressure rise due to deceleration is as high as 66 kPa, which is almost a half of the frictional pressure drop through the channel. Consequently, the channel pressure drop for this case is about 72 kPa only. Notably the inlet/outlet pressure loss for this case is also quite significant.

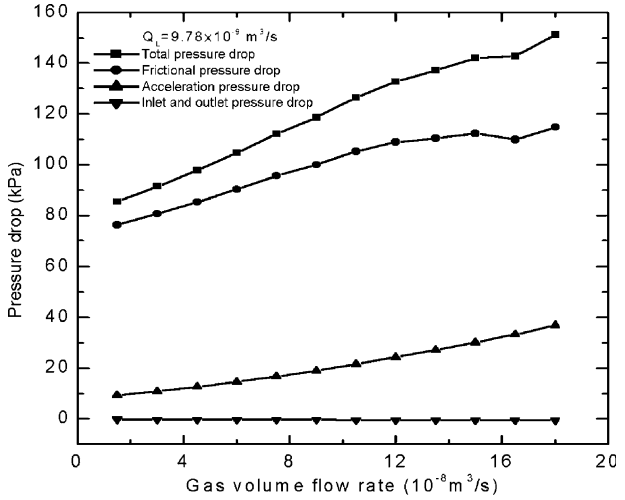

Fig. 13. Various components of two-phase pressure drops in the converging microchannel at $Q_L = 9.78 \times 10^{-9}$ m^3/s.

3.4. Correlations for two-phase frictional multiplier

The two-phase frictional pressure drop obtained in the present study may be employed to develop a correlation for a frictional multiplier in a converging or diverging channel. The two-phase frictional multiplier is defined as

$$\Phi_L^2 = \Delta P_{f,2P}/\Delta P_{f,L} \tag{19}$$

or

$$\Delta P_{f,2P} = \Phi_L^2 \Delta P_{f,L} \tag{20}$$

where $(\Delta P)_{f,L}$ is the frictional pressure drop for the liquid flowing alone through the same channel. Fig. 16(a) and (b) illustrate the two-phase frictional multiplier data against the Lockhart–Martinelli parameter and liquid flow rate in the converging and diverging microchannels, respectively. Both figures indicate that the multiplier can be correlated very well with the Lockhart–Martinelli parameter, while the liquid flow rate has a minor effect only on the multiplier. The insignificant effect of flow rate on two-phase frictional multiplier is consistent with that reported by Chung and Kawaji (2004), who found that the multiplier for uniform circular microchannels with diameter of 100 and 50 μm is quite independent of mass flux. Fig. 16(a) and (b) also show that the Lockhart–Martinelli equation with C value given by Mishima and Hibiki (See Eq. (2)) using the mean diameter of the channel significantly under-predicts the experimental data for both converging and diverging channels. If $C = 9.01$ from the best fit is adopted, the agreement with experimental data is within ±15% for the diverging channel. However, a similar approach for the converging microchannel results in poor prediction of experimental data as shown in Fig. 16(a). On the other hand, the data of the converging microchannel can be fitted very well if the C-value and the coefficient for X^{-2} in the Lockhart–Martinelli equation are best fitted as −2.64 and 47.5, respectively. Significantly, the ranges of flow rate for both phases warrant the flow

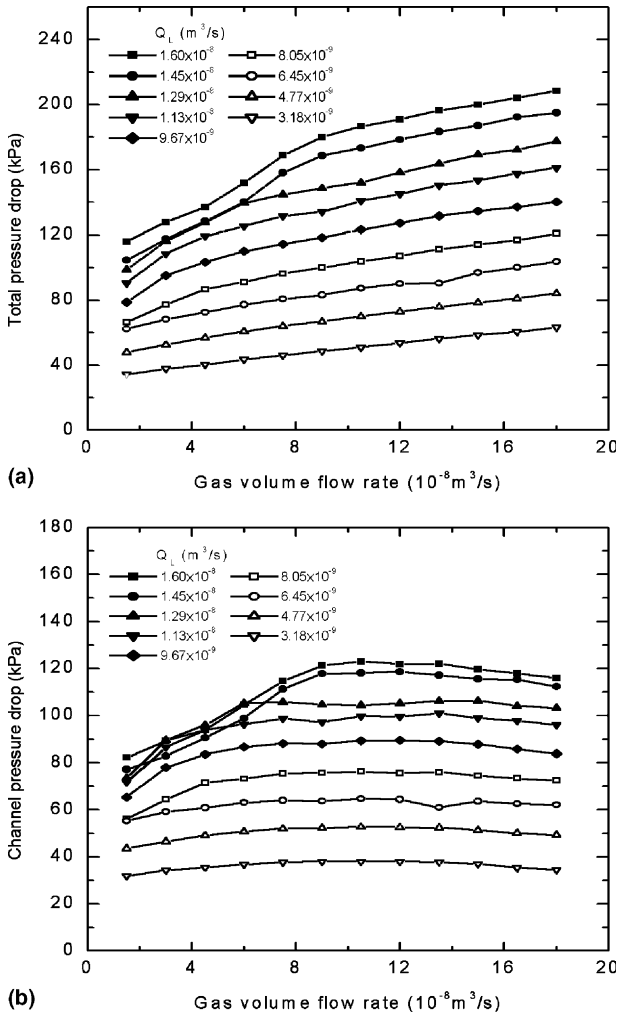

Fig. 14. Two-phase pressure drop in the diverging microchannel (a) total pressure drop, and (b) channel pressure drop.

for each phase alone will be laminar. Consequently, the Lockhart–Martinelli parameter may be expressed as

$$X = (\rho_G/\rho_L)(\mu_L/\mu_G)(1-x)/x \tag{21}$$

where x is the gas quality, as defined previously following Eq. (13).

4. Conclusions

Ethanol and CO_2 two-phase flow patterns and pressure drop in a converging or diverging rectangular microchannel were investigated experimentally. The following conclusions may be drawn from the results of this study.

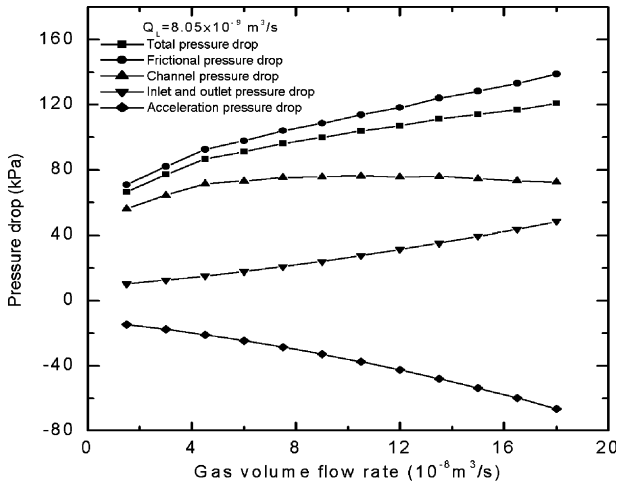

Fig. 15. Various components of two-phase pressure drops in the diverging microchannel at $Q_L = 8.05 \times 10^{-9}$ m^3/s.

1. The increased superficial gas velocity due to the acceleration effect and the large pressure drop in a converging microchannel may lead to the elongation of bubbles in slug flow. Annular flow may also be developed near the exit at high gas flow rate. Collisions and merger of two consecutive bubbles may occur and result in churn flow with necking bubbles. For high gas flow rates, stratified and wavy stratified flows appear at the entrance.
2. The decreased superficial gas velocity owing to the deceleration effect and the possible pressure rise in the diverging microchannel causes shortening of bubbles in slug flow significantly. For some cases with intermediate liquid flow rates, the bubble can become so short that the flow resembles bubbly flow. However, collision and merger of two consecutive bubbles also occur and result in the elongation or necking of bubbles. No annular flows were observed in the diverging channel.
3. The frictional factor for single-phase liquid flow may be predicted fairly well by the Hagen–Poiseuille equation with a constant of 160 for the converging microchannel and 91.4 for the diverging microchannel in the present study.
4. Two-phase flow pressure drop in the converging microchannel increases approximately linearly with the increasing liquid or gas flow rate. Both friction and acceleration contribute positively to the channel two-phase flow pressure drop with the friction component being the major contributor.
5. In the diverging microchannel, the deceleration effect results in the pressure rise and counteracts the frictional pressure drop. Consequently, for low liquid flow rates the channel pressure drop increases only slightly with the gas flow rate while it is low and a reversed trend appears while the gas flow rate is high. For high liquid flow rates the effect of increased gas flow rate on channel pressure drop is much more significant; a more significant reversed trend of the effect of gas flow rate is present in the region of high gas flow rates. Moreover, at a given gas flow rate, a higher liquid flow rate may actually result in a lower channel pressure drop.

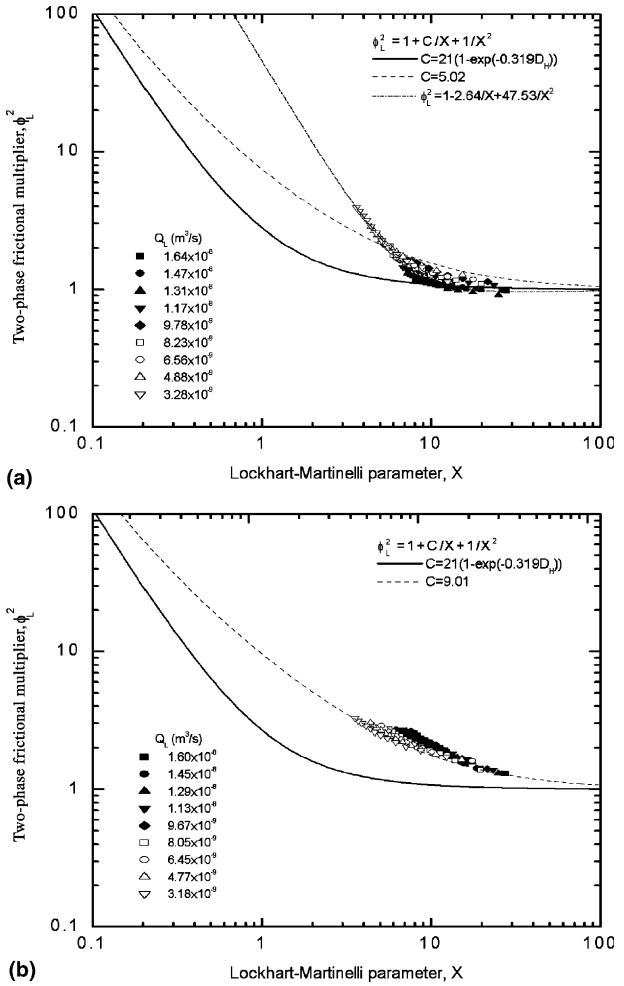

Fig. 16. Variation of two-phase frictional multiplier data with Lockhart–Martinelli parameter: (a) converging, (b) diverging microchannel.

6. The two-phase frictional multiplier in a converging or diverging microchannel is quite independent of liquid flow rate and can be fitted very well within ±15% with the Lockhart–Martinelli equation with a modified Chisholm parameter for the diverging microchannel and together with a modified coefficient for the X^{-2} term for the converging microchannel.

The results of the present study indicate that a diverging microchannel presents a significantly smaller channel pressure drop and, therefore, is much better than a converging channel for the transport of ethanol–CO_2 mixture. The implication of this study is that boiling heat transfer in a diverging microchannel could, in principle, offer high heat transfer capability and, yet, low two-phase flow pressure drop and is currently under study.

Acknowledgement

This work was supported by the National Science Council of Taiwan under the contract No. of NSC 92-2212-E-007-093. Mr. B. R. Fu helped re-plot all the figures and conduct the best fit of the frictional multiplier. His excellent efforts are highly appreciated.

References

Argyropulos, P., Scott, K., Taama, W.M., 1999. Gas evolution and power performance in direct methanol fuel cells. J. Appl. Electrochem. 29, 661–669.

Chen, W.L., Twu, M.C., Pan, C., 2002. Gas–liquid two-phase flow in micro-channels. Int. J. Multiphase Flow 28, 1235–1247.

Chung, P.M.-Y., Kawaji, M., 2004. The effect of channel diameter on adiabatic two-phase flow characteristics in microchannels. Int. J. Multiphase Flow 30, 735–761.

Collier, J.G., Thome, J.R., 1994. Convective Boiling and Condensation, third ed. Clarendon Press, Oxford, UK (Chapter 3).

Fukano, T., Kariyasaki, A., 1993. Characteristics of gas–liquid two-phase flow in capillary tube. Nucl. Eng. Design 141, 59–68.

Kawahara, A., Chung, P.M.-Y., Kawaji, M., 2002. Investigation of two phase flow pattern, void fraction and pressure drop in a Microchannel. Int. J. Multiphase Flow 28, 1411–1435.

Lee, P.C., Tseng, F.G., Pan, C., 2004. Bubble dynamics in microchannels, Part (I) single microchannel. Int. J. Heat Mass Transfer 47, 5575–5589.

Lin, L., Udell, K.S., Pisano, A.P., 1994. Liquid-vapor phase transition and bubble formation in micro structure. Thermal Sci. Eng. 2, 52–59.

Mishima, K., Hibiki, T., 1996. Some characteristics of air–water two–phase flow in small diameter vertical tubes. Int. J. Multiphase Flow 22, 703–712.

Serizawa, A., Feng, Z., Kawara, Z., 2002. Two-phase flow in microchannel. Exp. Thermal Fluid Sci. 26, 703–714.

Stanley, R.S., Barron, R.F., Ameel, T.A., 1997. Two-phase flow in micro channels. Microelectromech. Syst. ASME DSC-vol. 62/354.

Triplett, K.A., Ghiaasiaan, S.M., Abdel-Khalik, S.I., Sadowski, Sadowski, D.L., 1999a. Gas-liquid two-phase flow in microchannels, Part I: two-phase flow patterns. Int. J. Multiphase Flow 25, 377–394.

Triplett, K.A., Ghiaasiaan, S.M., Abdel-Khalik, S.I., Sadowski, Sadowski, D.L., 1999b. Gas–liquid two-phase flow in microchannels, Part II: void fraction and pressure drop. Int. J. Multiphase Flow 25, 395–410.

White, F.M., 1979. In: Fluid Mechanics. McGraw-Hill Book Co., New York, p. 356.

Yang, K.S., Chen, I.Y., Shew, B.Y., Wang, C.C., 2003. A Study of the fabrication and analysis of micro diffuser/nozzles. Proceedings of the 1st International Conference on Microchannels and Minichannels, paper number ICMM2003-1102, April 21–23, Rochester, New York, USA, 781–786.